

Magnetic field control of the excitonic transition in Ta_2NiSe_5

Giacomo Mazza

Dipartimento di Fisica dell'Università di Pisa, Largo Bruno Pontecorvo 3, I-56127 Pisa, Italy

The formation of excitonic insulator phases in quantum materials is often masked by structural distortions caused by the coupling between electronic and phononic order parameters. Here we show that the candidate material Ta_2NiSe_5 is characterized by a metastable excitonic insulating phase that is decoupled from the lattice, and that can be stabilized for sufficiently high applied magnetic fields. By considering the interplay between the excitonic and structural instabilities, we predict a magnetic field induced transition from the low-temperature structurally distorted semiconducting phase to an undistorted excitonic insulator phase with ground state loop currents. Before the transition, the existence of a latent excitonic phase can be detected by the magnetic field softening of the phonon mode associated with the structural distortion. These results highlight an unbiased route towards the disentanglement of the coupled excitonic-structural transition in Ta_2NiSe_5 , and uncover a general mechanism for magnetic field control of competing phases in quantum materials.

Introduction. Tunable metal-insulator transitions (MITs) have enormous potential for technological applications of quantum materials [1–3]. Often, MITs are interpreted as the distinctive signature of the formation of collective states of matter driven by strong electronic correlations, such as the Mott insulator state [4, 5]. However, in many correlated materials MITs occur simultaneously to structural distortions that mask the true microscopic origin of the MIT and, in turn, deeply alter the nature of the correlation-driven insulating states. In this context, the excitonic insulator (EI) state represents a paradigmatic example.

The EI is the particle-hole generalization of the superconducting paired state [6–9] occurring, for example, in bilayer systems with spatially separated particles and holes [10–15]. However, despite the many hints [16–23], the very existence of a bulk material hosting an EI phase remains a puzzle. In fact, the physical properties of the EI state are not unambiguously defined. Rather, the EI instability represents a general proxy for breaking some of the internal symmetries of a solid [24], so that there may exist many different EI states associated with different symmetry breaking channels [25–30]. In particular, the EI instability often involves the breaking of discrete symmetries of the crystal lattice, so that concurring structural distortions represent an inevitable obstacle in its identification.

Ta_2NiSe_5 is a candidate material in which the MIT has been associated to the formation of an EI state below a critical temperature, as suggested by the gap opening with characteristic flattening of the valence band around the Γ -point [16, 31, 32]. However, the EI transition is found to break the same crystal symmetries of the orthorombic-to-monoclinic lattice distortion [24, 33, 34] that occurs concomitantly to the MIT, stimulating an intense debate about the excitonic or structural origin of the low-temperature insulating phase [35]. So far, the various attempts to isolate the leading excitonic or structural character of the MIT, focussing, for example, on the analysis of collective excitations [36–46], have not led to a definite answer, and different conclusions can be found

in recent literature [47–49].

In this Letter, we propose a solution to the conundrum based on the stabilization of a latent EI phase immune to the lattice distortion. We show that, if the MIT in Ta_2NiSe_5 underlies an excitonic mechanism, the low-temperature structurally distorted phase can be transformed back into an undistorted EI by the application of

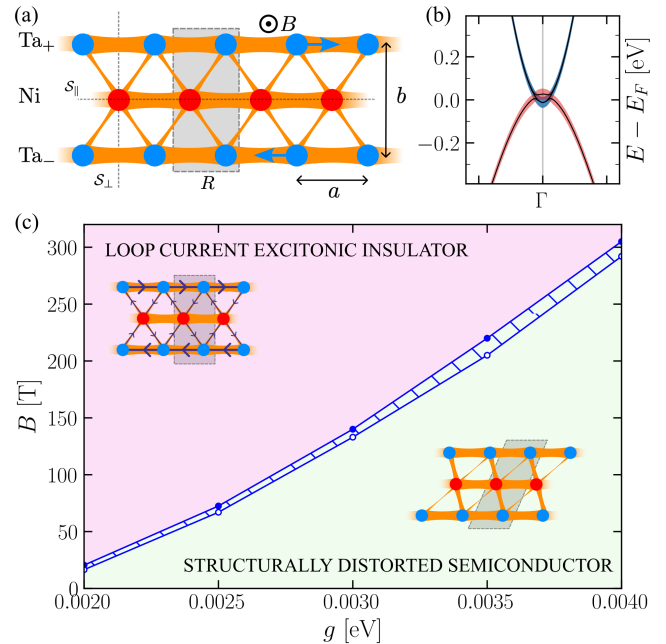


Figure 1. (a) Ta-Ni-Ta chain structure in the high-temperature orthorombic phase. The orange links schematically represent the charge distribution on the bonds. Shaded area highlights the unit cell. The blue arrows indicate the Ta-shear mode distortion. $a \approx 3.5 \text{ \AA}$ and $b \approx 3.9 \text{ \AA}$ are the lattice parameters of the chain. (b) Low-energy band structure for the high-temperature phase tight-binding model. Blue/red fat lines indicate the Ta/Ni characters of the bands. (c) Zero temperature phase diagram as a function of the perpendicular field B , and of the electron-phonon coupling g . The hatched area indicates a coexistence region.

a perpendicular magnetic field. Without magnetic field, the electron-coupling g drives the monoclinic distortion, and transforms the EI state into a simple, structurally distorted, semiconductor. For a field larger than a critical value $B > B_c$ the monoclinic distortion vanishes signalling the restoration of the orthorombic structure and the stabilization of an insulating phase characterized by closed current loops within the unit cell, see Fig. 1. Such a loop-current phase has a purely excitonic origin and it is related to the existence of a metastable EI phase which, in the absence of applied field, is destabilized by the electron-phonon coupling. In the whole structurally distorted region of the phase diagram, the latent loop current EI phase manifests through a field-induced suppression of the monoclinic distortion and the magnetic field softening of the phonon mode associated with the latter.

Excitonic phases and structural distortion. Ta_2NiSe_5 has a layered structure with each layer characterized by weakly coupled one-dimensional structures of alternating Ta-Ni-Ta chains, see Fig. 1(a). In the high-temperature phase, the unit cell is orthorombic and the system is metallic. The transition towards the low-temperature insulating phase is well described by a coupled excitonic-structural transition within a minimal model of interacting electrons in the Ta and Ni chains coupled to the Ta-shear mode [24, 33]. The full Hamiltonian, $H = H_{el} + H_{ph} + H_{el-ph}$, includes the purely electronic term $H_{el} = H_0 + H_{int}$, containing the tight-binding, H_0 , and density-density interaction, H_{int} , terms, the bare phonon Hamiltonian, H_{ph} , and the electron-phonon interaction, H_{el-ph} . Restricting, for simplicity, to a single Ta-Ni-Ta chain, the tight-binding Hamiltonian in the orthorombic phase reads

$$H_0 = \sum_{\sigma} \sum_{\alpha\beta} \sum_{RR'} t_{R,R'}^{\alpha\beta} c_{R\alpha\sigma}^{\dagger} c_{R'\beta\sigma}, \quad (1)$$

where $c_{R\alpha\sigma}^{\dagger}/c_{R\alpha\sigma}$ are creation/annihilation operators for electrons with spin σ in the Wannier orbitals localized on the atom α in the unit cell R containing an upper (Ta₊) and a lower (Ta₋) Ta-atom and a central Ni-atom. In the following, we truncate the hoppings at the nearest-neighboring atoms, and fix $t_{R,R+a}^{\text{Ta+},\text{Ta+}} = t_{R,R+a}^{\text{Ta-},\text{Ta-}} = -0.72$ eV, $t_{R,R+a}^{\text{Ni},\text{Ni}} = 0.3$ eV, $t_{R,R}^{\text{Ta+},\text{Ta+}} = t_{R,R}^{\text{Ta-},\text{Ta-}} = 2.0$ eV, $t_{R,R}^{\text{Ni},\text{Ni}} = 0$ eV, and $t_{R,R}^{\text{Ta±},\text{Ni}} = -t_{R,R-a}^{\text{Ta±},\text{Ni}} = 35$ meV, obtaining a low-energy band structure characterized by weakly overlapping conduction and valence bands of predominant Ta- and Ni-characters respectively, see Fig. 1(b). The density-density interaction reads

$$H_{int} = \sum_{\sigma\sigma'} \sum_{\alpha\beta} \sum_{RR'} U_{\alpha\beta}^{\sigma\sigma'} (R - R') c_{R\alpha\sigma}^{\dagger} c_{R\alpha\sigma} c_{R'\beta\sigma'}^{\dagger} c_{R'\beta\sigma'}, \quad (2)$$

where $U_{\alpha\beta}^{\sigma\sigma'}(R - R')$ are long-range interaction potentials parametrized by local intra- and inter-chain interaction

strengths $U_{\alpha} \equiv U_{\alpha\alpha}^{\sigma-\sigma}(R = R')$, $V \equiv U_{\text{Ta}\pm,\text{Ni}}^{\sigma\sigma'}(R = R')$, where we neglected inter-chain Ta₊ – Ta₋ interactions. The bare phonon Hamiltonian reads $H_{ph} = \hbar\omega_0 \sum_R \sum_{\alpha=\text{Ta}\pm} b_{R\alpha}^{\dagger} b_{R\alpha}$, where $b_{\text{Ta}\pm R}^{\dagger}/b_{\text{Ta}\pm R}$ are bosonic creation/annihilation operators describing the vibration of the Ta_±-atoms along the chains. Finally, the electron-phonon Hamiltonian $H_{el-ph} = \sum_{\alpha=\text{Ta}\pm} H_{el-ph}^{\alpha}$ includes the linear coupling between Ta_± displacement and the Ta_±-Ni nearest neighbour hybridization as

$$H_{el-ph}^{\alpha} = g \sum_{R\sigma} X_{R\alpha} \left(c_{R\text{Ni}\sigma}^{\dagger} c_{R\alpha\sigma} + c_{R\text{Ni}\sigma}^{\dagger} c_{R-a\alpha\sigma} + \text{h.c.} \right), \quad (3)$$

with $X_{R\pm} \equiv b_{R\pm}^{\dagger} + b_{R\pm}$ and g is a dimensional electron-phonon coupling.

We solve the electron-phonon model using the mean-field decoupling $|\Psi\rangle = |\Psi_{el}\rangle|\Psi_{ph}\rangle$, where $|\Psi_{el}\rangle$ and $|\Psi_{ph}\rangle$ are self-consistently determined as the ground states of effective purely electronic, \tilde{H}_{el} , and phononic, \tilde{H}_{ph} , Hamiltonians obtained upon averaging the full Hamiltonian over the phononic and electronic wavefunctions, respectively. The electronic part is treated using a standard Hartree-Fock (HF) decoupling of the density-density interaction in the particle-hole channel by fixing the average number of electrons per unit cell $n_R = \sum_{\alpha\sigma} \langle c_{R\alpha\sigma}^{\dagger} c_{R\alpha\sigma} \rangle = 2$, see [50] for details. In the following, we choose model parameters allowing for an excitonic instability. We fix the intra-chain interaction parameters $U_{\text{Ni}} = 1.5$ eV, $U_{\text{Ta}\pm} = 0.5$ eV and the bare phonon energy $\hbar\omega_0 = 10$ meV, and vary the inter-chain interaction parameter V and the electron-phonon coupling g . Different choices of the model parameters do not alter the qualitative picture described in this work.

Let us first set $g = 0$, and consider the purely excitonic instability. The EI instability is related to the breaking of the reflection symmetry with respect to the transverse plane \mathcal{S}_{\perp} which constrains the hybridization between Ta- and Ni-Wannier orbitals to vanish at the Γ -point. This implies the existence of a two-components complex order parameter

$$\Psi_{\text{EI}} = (\Psi_+, \Psi_-), \text{ with } \Psi_{\pm} \equiv \sum_{\sigma} \langle c_{k=0\text{Ta}\pm\sigma}^{\dagger} c_{k=0\text{Ni}\sigma} \rangle, \quad (4)$$

and $c_{k\alpha\sigma} \equiv \frac{1}{N} \sum_R e^{ikR} c_{R\alpha\sigma}$, which is zero in the orthorombic phase, and becomes $\Psi_{\text{EI}} \neq 0$ due to a spontaneous conduction/valence band hybridization triggered by the excitonic instability. We assume that the instability preserves the symmetry of the low-temperature monoclinic phase. This choice fixes $\Psi_+ = -\Psi_- = \Psi$, and reduces the order parameter to a single complex number $\Psi = |\Psi|e^{i\varphi}$.

We solve the self-consistent HF problem at zero-temperature by seeding a non-zero excitonic order parameter in the complex plane with different phases. For an interaction parameter larger than a critical value $V \gtrsim 0.8$ eV, we find that symmetry breaking can either occur with a purely real, $\varphi = 0$, or purely imagi-

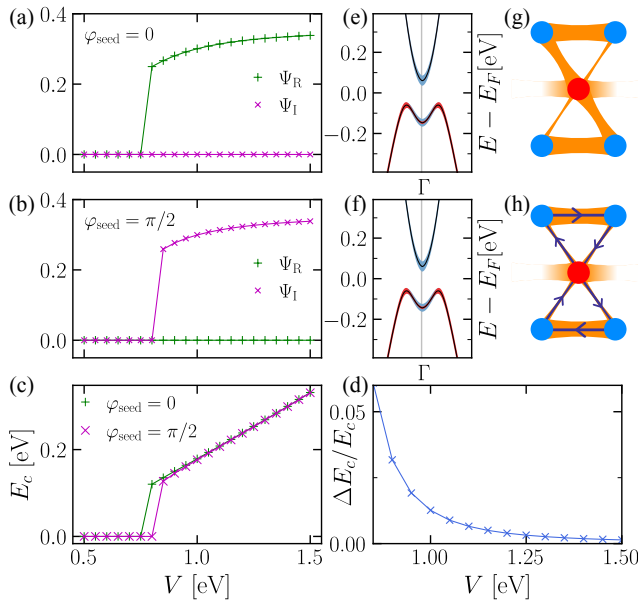


Figure 2. (a)-(b) Real Ψ_R and imaginary Ψ_I parts of the excitonic order parameter obtained using seeds $\Psi_{\text{seed}} = 0.2e^{i\varphi_{\text{seed}}}$ with $\varphi_{\text{seed}} = 0$ (a) and $\varphi_{\text{seed}} = \pi/2$ (b). (c) Condensation energies for the $\varphi = 0$ and $\varphi = \pi/2$ phases. (d) Relative energy difference $\Delta E_c = E_c(\varphi = 0) - E_c(\varphi = \pi/2)$ normalized to $E_c(0)$. (e)-(f) Low-energy bands in the $\varphi = 0$ (e) and $\varphi = \pi/2$ (f) cases at $V = 1.0$ eV (g)-(h) Sketches of the charge density and the bond current distributions in the $\varphi = 0$ (g) and $\varphi = \pi/2$ (h) phases.

nary, $\varphi = \pi/2$, order parameters, see Fig. 2(a)-(b). In panels (c)-(d), we compare the condensation energies, $E_c(\Psi) \equiv E(\Psi = 0) - E(\Psi) > 0$, of the two phases showing that $E_c(\varphi = 0) > E_c(\varphi = \pi/2)$ from which we identify the stable ($\varphi = 0$) and metastable ($\varphi = \pi/2$) excitonic phases.

Notably, the two phases are essentially indistinguishable from a band structure point of view. In both cases, the symmetry breaking results in the opening of a slightly indirect gap which, for $V = 1.0$ eV, is ~ 0.1 eV. However, by considering a symmetry analysis of charge and current densities, one can show that the two EI phases correspond to two strikingly different physical states. In fact, the order parameter controls the hybridization between neighbouring Wannier orbitals and, since the latter are real, the real and imaginary parts of the hybridization affect, respectively, the charge and current densities on the bonds between two Wannier centers, see [50]. Specifically, the $\varphi = 0$ state corresponds to the usual charge distorted configuration of Ta_2NiSe_5 [24, 34] characterized by a charge density asymmetry on the neighboring $\text{Ta}_{\pm}\text{-Ni}$ bonds, see Fig. 2(g). Remarkably, for $\varphi = \pi/2$ the charge density preserves the symmetries of the orthorombic phase whereas the symmetry breaking results in the formation of a loop current pattern on the $\text{Ta}_{\pm}\text{-Ni}$ and $\text{Ta}_{\pm}\text{-Ta}_{\pm}$ bonds, see Fig. 2(h). We therefore dub the stable and metastable phases as the charge distorted (CD)

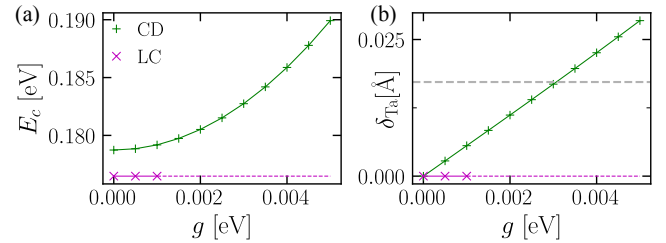


Figure 3. (a) Condensation energy of the CD and LC phases as a function of the dimensional electron-phonon coupling. (b) Displacement of the Ta-atom with respect to the equilibrium position in the orthorombic phase. For the LC phase, the dashed lines indicate that, for the corresponding values of g , the solution is unstable.

and the loop current (LC) excitonic phases, respectively. We notice that the difference in the condensation energies of these extremely different symmetry broken phases can be relatively small, see Fig. 2(d). Despite this, any possible energetic competition between the two phases is eventually overruled by the interaction with the Ta-chains shear mode which, by coupling with the charge density, drives the monoclinic distortion. In Fig. 3(a), we show the condensation energy of the CD and LC phases for $V = 1.0$ eV, and as a function of the electron-phonon coupling g . As expected, the coupling with phonons enhances the stability of the CD phase, and induces a static monoclinic distortion $\langle X_{R+} \rangle = -\langle X_{R-} \rangle \neq 0$ that grows linearly with g , Fig. 3(b). We give a rough estimate of the corresponding Ta-atom displacement δ_{Ta} by setting $\delta_{\text{Ta}} = \ell_0 \langle X_{R+} \rangle$ with $\ell_0 = \sqrt{\hbar/(2M_{\text{Ta}}\omega_0)} \approx 0.03$ Å, being M_{Ta} the mass of the Ta-ion, and obtain a distortion which, in the range 2 meV $\lesssim g \lesssim 5$ meV, is of the same order of magnitude of the observed monoclinic distortion with angle $\sim 0.5^\circ$ [31]. On the contrary, the coupling with phonons destroys the LC phase. For small values of g , the LC phase exists as a metastable undistorted phase with a g -independent condensation energy. However, as revealed by a fluctuation analysis about the equilibrium mean-field solution [50], we observe that the LC undistorted phase becomes quickly unstable upon increasing g , and completely disappears for $g \gtrsim 1.5$ meV.

Field-induced stabilization of the undistorted EI phase. Despite the fact that the electron-phonon coupling destroys the LC phase for $g \gtrsim 1.5$ meV, the very existence of a metastable LC state for $g = 0$ suggests that it may be possible to counterbalance the detrimental effects of the coupling to the lattice by using a perpendicular magnetic field. We include a constant magnetic field, B , via Peierls phases in the hoppings [51–53]

$$t_{R,R'}^{\alpha\beta} \rightarrow t_{R,R'}^{\alpha\beta} e^{i\phi_{R,R'}^{\alpha,\beta}/\Phi_0}, \quad (5)$$

with $\Phi_0 \equiv \frac{\hbar}{e}$, and consider a Zeeman coupling with g-factor $g_s = 2$. The Peierls phases are defined in terms of the flux through the $\text{Ta}_{\pm}\text{-Ni-Ta}_{\pm}\text{-Ni}$ diamond-like plaquette $\Phi_{\diamond} = BA_{\diamond}$, with $A_{\diamond} = ab \simeq 0.14$ nm².

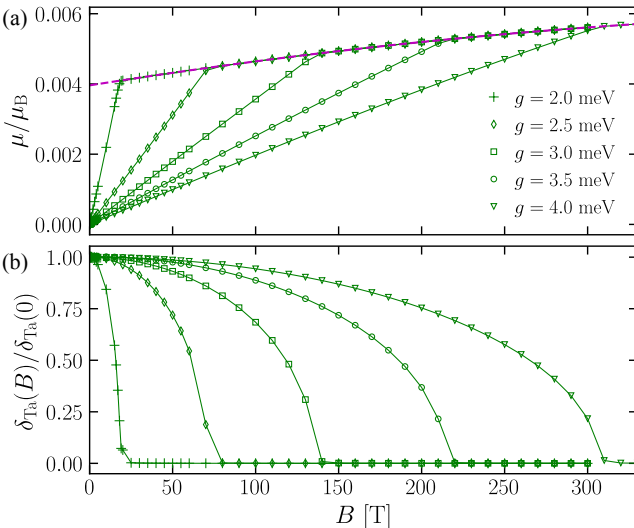


Figure 4. (a) Orbital magnetic moment as a function of the applied magnetic field B , and for different values of g . The dashed magenta lines corresponds to the magnetic moment of the LC phase obtained by imposing $\delta_{\text{Ta}} = 0$. (b) Static displacement of the Ta-atoms as a function of the applied fields and the same values of g shown in (a).

We fix the relative phases by imposing $\Phi_\diamond = 2\Phi_\nabla = 2\Phi_\triangle$, Φ_∇/\triangle being the fluxes threading the upper ($\text{Ta}_+ \text{-} \text{Ni} \text{-} \text{Ta}_+$)/lower ($\text{Ta}_- \text{-} \text{Ni} \text{-} \text{Ta}_-$) triangular plaquettes, and obtain $\phi_{R,R}^{\text{Ta}_+ \text{Ni}} = \frac{\Phi_\diamond}{4}$, $\phi_{R-a,R}^{\text{Ta}_+ \text{Ni}} = -\frac{\Phi_\diamond}{4}$, $\phi_{R+a,R}^{\text{Ta}_+ \text{Ta}_+} = -\phi_{R+a,R}^{\text{Ta}_- \text{Ta}_-} = \Phi_\diamond$, and $\phi_{R+a,R}^{\text{NiNi}} = 0$.

For all the considered values of B the Zeeman splitting is smaller than the gap of the structurally distorted phase and the spin magnetic moment is always zero. In contrast, the magnetic field induces a finite orbital magnetic moment which we define as $\vec{\mu} = \int d\vec{r} \vec{r} \times \vec{j}(\vec{r})$, where \vec{r} is the vector originating from the Ni-atom of the $R = 0$ cell, and $\vec{j}(\vec{r})$ the current density defined on the links [50].

In Fig. 4(a), we plot μ as a function of the applied field and different values of g . The orbital magnetic moment increases linearly with B with a paramagnetic susceptibility inversely proportional to g . At a g -dependent critical value B_c , the magnetization curves show a kink and, for $B > B_c$, they all merge into a single g -independent curve. Remarkably, the magnetic moment increase is accompanied by a suppression of the shear mode displacement, Fig. 4(b). The distortion continuously goes to zero at B_c showing that sufficiently high magnetic fields can revert the orthorombic-to-monoclinic distortion.

It is immediate to check that the field-induced restoration of the orthorombic symmetry coincides with the stabilization of the previously discussed LC excitonic phase. Starting from the undistorted phase at high fields, we follow the orbital magnetization backwards by constraining $\delta_{\text{Ta}} = 0$, and observe an hysteretic-like behaviour (dashed line) converging to the purely excitonic LC phase for $B = 0$. We stress that this is not a truly hysteretic

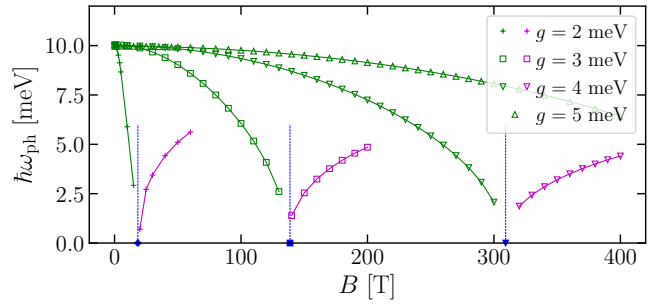


Figure 5. Phonon frequency as a function of the magnetic field and different values of electron-phonon coupling, and $V = 1.0$ eV. For each g , the green and magenta symbols corresponds, respectively, to the structurally distorted semiconductor and LC excitonic insulator phase. The dots and the vertical dashed lines indicate the critical fields B_c .

behavior since, as already mentioned, the LC phase at $B = 0$ is unstable for $g \gtrsim 1.5$ meV. However, by carrying out the fluctuation analysis at finite B , we observe that, for all values of g , the stability of the LC phase is eventually recovered for $B > B_*$, with $B_* \lesssim B_c$, leading to a coexistence region close to the transition line, see Fig. 1.

Having shown the field-induced stabilization of the undistorted LC phase, we now discuss detection of the latent LC phase by means of dynamical phonon response. We compute the phonon spectral functions $A_{\text{ph}}(\omega)$ using time-dependent HF and extract the phonon frequency as $\omega_{\text{ph}} \equiv \int d\omega A_{\text{ph}}(\omega) \omega / \int d\omega A_{\text{ph}}(\omega)$. In Fig. 5, we report the phonon frequency dependence as a function of B and increasing values of g . The phonon mode shows a clear magnetic field softening, $\partial\omega_{\text{ph}}/\partial B < 0$, for $B < B_c$, ending up in a complete softening $\omega_{\text{ph}} \rightarrow 0$ as $B \rightarrow B_c$. Eventually, the mode softening is followed by a phonon hardening, $\partial\omega_{\text{ph}}/\partial B > 0$, for $B > B_c$. This shows that the phonon response may detect the latent LC phase even even for fields smaller than B_c , thus providing a clear-cut criterion for the determination of the dominant mechanism underlying the MIT. Specifically, if the dominant mechanisms is excitonic, we expect to detect the latent EI phase by a strong a strong magnetic field softening of the phonon mode. On the contrary, if the monoclinic distortion is dominated by the effects electron-phonon coupling, we expect a negligible field response of the lattice.

Conclusion. We have shown that the excitonic instability in Ta_2NiSe_5 is characterized by an undistorted LC phase whose stability is controlled by the competing effects of the electron-phonon coupling and of the applied magnetic field. We predict that the application of a perpendicular magnetic field suppresses the monoclinic distortion and, for sufficiently high fields, leads to the restoration of the orthorombic symmetry and the stabilization of the LC excitonic phase, leading to an effective decoupling of the excitonic and structural transitions.

Critical fields for the stabilization of the undistorted LC phase are expected to be of the order of few hundreds of Tesla. Tunability of MITs under such ultra-high fields has been already explored, for example, in vanadium oxides [54]. Nonetheless, the excitonic nature of the Ta_2NiSe_5 low-temperature phase may be revealed at fields much smaller than the critical one through the investigation of the magnetic field response of the lattice dynamics.

Besides being directly relevant in the case of Ta_2NiSe_5 , the mechanism for the emergence of LC phase due to

interaction-driven spontaneous hybridization can be very general. In this respect, these results highlight the interplay between strongly correlated phases with spontaneous orbital currents and the electron-lattice coupling as a promising route for the control of exotic phases in quantum materials.

Acknowledgments. I thank M. Rosner, A. Millis, A. Georges, A. Amaricci, M. Capone, and M. Polini for discussions. I am grateful to A. Amaricci for critical reading of the manuscript. This work received funding from the MUR, Italian Minister of University and Research, through a “Rita Levi-Montalcini” fellowship.

[1] Y. Tokura, M. Kawasaki, and N. Nagaosa, *Nature Physics* **13**, 1056 (2017).

[2] Z. Wang, H. Wu, G. W. Burr, C. S. Hwang, K. L. Wang, Q. Xia, and J. J. Yang, *Nature Reviews Materials* **5**, 173 (2020).

[3] J. del Valle, J. G. Ramirez, M. J. Rozenberg, and I. K. Schuller, *Journal of Applied Physics* **124**, 211101 (2018).

[4] M. Imada, A. Fujimori, and Y. Tokura, *Rev. Mod. Phys.* **70**, 1039 (1998).

[5] N. F. Mott, *Proceedings of the Physical Society. Section A* **62**, 416 (1949).

[6] D. Jérôme, T. M. Rice, and W. Kohn, *Phys. Rev.* **158**, 462 (1967).

[7] A. N. Kozlov and L. A. Maksimov, *Soviet Journal of Experimental and Theoretical Physics* **21**, 790 (1965).

[8] B. I. Halperin and T. M. Rice, *Rev. Mod. Phys.* **40**, 755 (1968).

[9] L. V. Keldysh and A. N. Kozlov, *Soviet Journal of Experimental and Theoretical Physics* **27**, 521 (1968).

[10] I. B. Spielman, J. P. Eisenstein, L. N. Pfeiffer, and K. W. West, *Phys. Rev. Lett.* **84**, 5808 (2000).

[11] M. Kellogg, J. P. Eisenstein, L. N. Pfeiffer, and K. W. West, *Phys. Rev. Lett.* **93**, 036801 (2004).

[12] J. P. Eisenstein and A. H. MacDonald, *Nature* **432**, 691 (2004).

[13] J. Eisenstein, *Annual Review of Condensed Matter Physics* **5**, 159 (2014), <https://doi.org/10.1146/annurev-conmatphys-031113-133832>.

[14] L. Ma, P. X. Nguyen, Z. Wang, Y. Zeng, K. Watanabe, T. Taniguchi, A. H. MacDonald, K. F. Mak, and J. Shan, *Nature* **598**, 585 (2021).

[15] P. X. Nguyen, R. Chaturvedi, B. Zou, K. Watanabe, T. Taniguchi, A. H. MacDonald, K. F. Mak, and J. Shan, *Nature Materials* (2025), 10.1038/s41563-025-02334-3.

[16] Y. F. Lu, H. Kono, T. I. Larkin, A. W. Rost, T. Takayama, A. V. Boris, B. Keimer, and H. Takagi, *Nat. Commun.* **8**, 14408 (2017).

[17] A. Kogar, M. S. Rak, S. Vig, A. A. Husain, F. Flicker, Y. I. Joe, L. Venema, G. J. MacDougall, T. C. Chiang, E. Fradkin, J. van Wezel, and P. Abbamonte, *Science* **358**, 1314 (2017), <http://science.scienmag.org/content/358/6368/1314.full.pdf>.

[18] D. Varsano, M. Palummo, E. Molinari, and M. Rontani, *Nature Nanotechnology* **15**, 367 (2020).

[19] S. S. Ataei, D. Varsano, E. Molinari, and M. Rontani, *Proceedings of the National Academy of Sciences* **118**, e2010110118 (2021), <https://www.pnas.org/doi/pdf/10.1073/pnas.2010110118>.

[20] Y. Jia, P. Wang, C.-L. Chiu, Z. Song, G. Yu, B. Jäck, S. Lei, S. Klemenz, F. A. Cevallos, M. Onyszczak, N. Fishchenko, X. Liu, G. Farahi, F. Xie, Y. Xu, K. Watanabe, T. Taniguchi, B. A. Bernevig, R. J. Cava, L. M. Schoop, A. Yazdani, and S. Wu, *Nature Physics* **18**, 87 (2022).

[21] B. Sun, W. Zhao, T. Palomaki, Z. Fei, E. Runburg, P. Malinowski, X. Huang, J. Cenker, Y.-T. Cui, J.-H. Chu, X. Xu, S. S. Ataei, D. Varsano, M. Palummo, E. Molinari, M. Rontani, and D. H. Cobden, *Nature Physics* **18**, 94 (2022).

[22] J. Mei, Y. Wang, R. Fei, J. Wang, X. Gan, B. Liu, and X. Wang, *Nature Communications* **16**, 3744 (2025).

[23] M. S. Hossain, Z.-J. Cheng, Y.-X. Jiang, T. A. Cochran, S.-B. Zhang, H. Wu, X. Liu, X. Zheng, G. Cheng, B. Kim, Q. Zhang, M. Litskevich, J. Zhang, J. Liu, J.-X. Yin, X. P. Yang, J. D. Denlinger, M. Tallarida, J. Dai, E. Vescovo, A. Rajapitamahuni, N. Yao, A. Keselman, Y. Peng, Y. Yao, Z. Wang, L. Balicas, T. Neupert, and M. Z. Hasan, *Nature Physics* **21**, 1250 (2025).

[24] G. Mazza, M. Rösner, L. Windgärtter, S. Latini, H. Hübener, A. J. Millis, A. Rubio, and A. Georges, *Phys. Rev. Lett.* **124**, 197601 (2020).

[25] G. Mazza and M. Polini, *Phys. Rev. B* **108**, L241107 (2023).

[26] Y.-Q. Wang, M. Papaj, and J. E. Moore, *Phys. Rev. B* **108**, 205420 (2023).

[27] A. Amaricci, G. Mazza, M. Capone, and M. Fabrizio, *Phys. Rev. B* **107**, 115117 (2023).

[28] M. Papaj, *Phys. Rev. B* **110**, 165422 (2024).

[29] V.-N. Phan, *Phys. Rev. B* **112**, L201110 (2025).

[30] N. Ohta and J. Nasu, *Journal of the Physical Society of Japan* **94**, 054702 (2025), <https://doi.org/10.7566/JPSJ.94.054702>.

[31] F. D. Salvo, C. Chen, R. Fleming, J. Waszczak, R. Dunn, S. Sunshine, and J. A. Ibers, *Journal of the Less Common Metals* **116**, 51 (1986).

[32] K. Seki, Y. Wakisaka, T. Kaneko, T. Toriyama, T. Konishi, T. Sudayama, N. L. Saini, M. Arita, H. Namatame, M. Taniguchi, N. Katayama, M. Nohara, H. Takagi, T. Mizokawa, and Y. Ohta, *Phys. Rev. B* **90**, 155116 (2014).

[33] T. Kaneko, T. Toriyama, T. Konishi, and Y. Ohta, *Phys. Rev. B* **87**, 035121 (2013).

- [34] M. D. Watson, I. Marković, E. A. Morales, P. Le Fèvre, M. Merz, A. A. Haghhighirad, and P. D. C. King, *Phys. Rev. Research* **2**, 013236 (2020).
- [35] A. Fujimori, *Journal Club for Condensed Matter Physics* (2020), 10.36471/JCCM_August_2020_01.
- [36] D. Werdehausen, T. Takayama, M. Höppner, G. Albrecht, A. W. Rost, Y. Lu, D. Manske, H. Takagi, and S. Kaiser, *Science Advances* **4** (2018), 10.1126/sciadv.aap8652, <http://advances.sciencemag.org/content/4/3/eaap8652.full.pdf>.
- [37] D. Golež, Z. Sun, Y. Murakami, A. Georges, and A. J. Millis, *Phys. Rev. Lett.* **125**, 257601 (2020).
- [38] K. Kim, H. Kim, J. Kim, C. Kwon, J. S. Kim, and B. J. Kim, *Nature Communications* **12**, 1969 (2021).
- [39] M. Ye, P. A. Volkov, H. Lohani, I. Feldman, M. Kim, A. Kanigel, and G. Blumberg, *Phys. Rev. B* **104**, 045102 (2021).
- [40] A. Subedi, *Phys. Rev. Mater.* **4**, 083601 (2020).
- [41] L. Windgäetter, M. Rösner, G. Mazza, H. Hübener, A. Georges, A. J. Millis, S. Latini, and A. Rubio, *npj Computational Materials* **7**, 210 (2021).
- [42] P. A. Volkov, M. Ye, H. Lohani, I. Feldman, A. Kanigel, and G. Blumberg, *npj Quantum Materials* **6**, 52 (2021).
- [43] D. Golež, S. K. Y. Dufresne, M.-J. Kim, F. Boschini, H. Chu, Y. Murakami, G. Levy, A. K. Mills, S. Zhdanovich, M. Isobe, H. Takagi, S. Kaiser, P. Werner, D. J. Jones, A. Georges, A. Damascelli, and A. J. Millis, *Phys. Rev. B* **106**, L121106 (2022).
- [44] J. Chen, J. Mravlje, D. Golež, and P. Werner, “2d coherent spectroscopy signatures of exciton condensation in ta_2nise_5 ,” (2025), arXiv:2512.19689 [cond-mat.str-el].
- [45] K. Katsumi, A. Alekhin, S.-M. Souliou, M. Merz, A.-A. Haghhighirad, M. Le Tacon, S. Houver, M. Cazayous, A. Sacuto, and Y. Gallais, *Phys. Rev. Lett.* **130**, 106904 (2023).
- [46] E. Baldini, A. Zong, D. Choi, C. Lee, M. H. Michael, L. Windgaetter, I. I. Mazin, S. Latini, D. Azoury, B. Lv, A. Kogar, Y. Su, Y. Wang, Y. Lu, T. Takayama, H. Takagi, A. J. Millis, A. Rubio, E. Demler, and N. Gedik, *Proceedings of the National Academy of Sciences* **120**, e2221688120 (2023), <https://www.pnas.org/doi/pdf/10.1073/pnas.2221688120>.
- [47] K. Wei, Y. Luo, K. Watanabe, T. Taniguchi, Y. Guo, and X. Xi, *Nature Communications* **16**, 10999 (2025).
- [48] E. Rosenberg, J. Ayres-Sims, A. Millis, D. Cobden, and J.-H. Chu, “Elastocaloric signature of the excitonic instability in ta_2nise_5 ,” (2025), arXiv:2504.10837 [cond-mat.str-el].
- [49] S. Bae, A. Raghavan, I. Feldman, A. Kanigel, and V. Madhavan, “Microscopic evidence of dominant excitonic instability in ta_2nise_5 ,” (2025), arXiv:2512.03011 [cond-mat.str-el].
- [50] See Supplemental Material containing details on the model Hamiltonian.
- [51] R. Peierls, *Zeitschrift für Physik* **80**, 763 (1933).
- [52] J. M. Luttinger, *Phys. Rev.* **84**, 814 (1951).
- [53] J. Li, D. Golež, G. Mazza, A. J. Millis, A. Georges, and M. Eckstein, *Phys. Rev. B* **101**, 205140 (2020).
- [54] Y. H. Matsuda, D. Nakamura, A. Ikeda, S. Takeyama, Y. Suga, H. Nakahara, and Y. Muraoka, *Nature Communications* **11**, 3591 (2020).

Supplemental Information:

Magnetic field control of the excitonic transition in Ta_2NiSe_5

Giacomo Mazza

Dipartimento di Fisica dell'Università di Pisa, Largo Bruno Pontecorvo 3, I-56127 Pisa, Italy

I. Model Hamiltonian and mean-field decoupling	1
II. Charge and current density	3
Charge Density	3
Current Density	4
III. Electron phonon coupling and stability of the LC phase	5
IV. Lattice dynamics	7
References	7

I. MODEL HAMILTONIAN AND MEAN-FIELD DECOUPLING

The electronic Hamiltonian considered in the paper is

$$H_{el} = H_0 + H_{int} \quad (1)$$

where H_0 is the tight-binding Hamiltonian and H_{int} contains density-density interaction terms. The tight-binding Hamiltonian is built from Wannier orbitals localized on the upper and lower Ta-atoms and on the central Ni-atom, and it reads

$$H_0 = \sum_{\sigma} \sum_{\alpha\beta}^{\{\text{Ta}_{\pm}, \text{Ni}\}} \sum_{RR'} t_{R,R'}^{\alpha\beta} c_{R\alpha\sigma}^{\dagger} c_{R'\beta\sigma}. \quad (2)$$

We recall the symmetries of the Ta_2NiSe_5 tight-binding Hamiltonian referring the reader to Ref. [1] for an in-depth discussion. The Ta- and Ni- Wannier orbitals are, respectively, even and odd with respect to the reflections about the the transverse plane \mathcal{S}_{\perp} . Specifically, by indicating with (x, y) the spatial coordinates of the chain plane with origin $x = 0$ and $y = 0$ on the Ni-atom of the $R = 0$ cell, and \mathcal{S}_{\perp} the $x = 0$ plane, the Wannier orbitals centred on the atom α of the cell R , $w_{\alpha,R}(x, y)$, transform under reflections about the \mathcal{S}_{\perp} plane according to

$$\begin{aligned} w_{R, \text{Ta}_{\pm}}(x, y) &= w_{-R-a, \text{Ta}_{\pm}}(-x, y) \\ w_{R, \text{Ni}}(x, y) &= -w_{-R, \text{Ni}}(-x, y). \end{aligned} \quad (3)$$

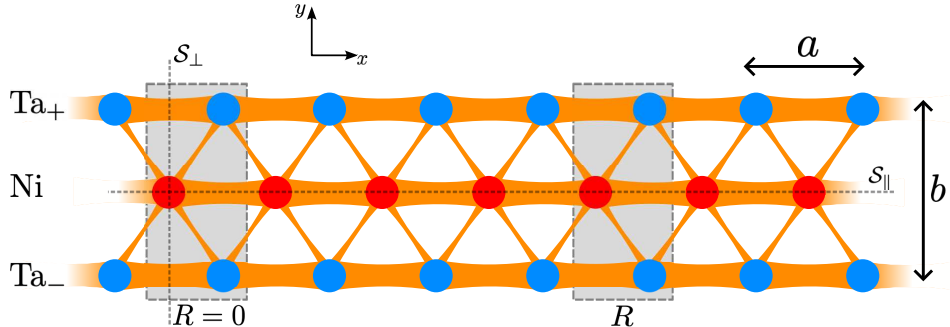


Figure 1. Chain structure of Ta_2NiSe_5 in the orthorhombic phase.

By considering reflections about the $y = 0$ plane (\mathcal{S}_{\parallel})

$$\begin{aligned} w_{R,\text{Ta}\pm}(x, y) &= w_{R,\text{Ta}\mp}(x, -y) \\ w_{R,\text{Ni}}(x, y) &= w_{R,\text{Ni}}(x, -y). \end{aligned} \quad (4)$$

This reflection symmetries constraint the hopping parameters describing the $\text{Ta}_{\pm} - \text{Ni}$ hybridization as

$$t_{R,R}^{\text{Ta}\pm\text{Ni}} = -t_{R,R-a}^{\text{Ta}\pm\text{Ni}}. \quad (5)$$

Analogously, we define the transformation of the fermionic operators under the reflection symmetries $\mathcal{R}_{\mathcal{S}_{\perp}}$ and $\mathcal{R}_{\mathcal{S}_{\parallel}}$ as

$$\begin{aligned} \mathcal{R}_{\mathcal{S}_{\perp}} c_{R,\text{Ta}\pm\sigma}^{\dagger} &\rightarrow c_{-R-a,\text{Ta}\pm\sigma}^{\dagger} \\ \mathcal{R}_{\mathcal{S}_{\perp}} c_{R,\text{Ni}\sigma}^{\dagger} &\rightarrow -c_{-R,\text{Ni}\sigma}^{\dagger}, \end{aligned} \quad (6)$$

and

$$\begin{aligned} \mathcal{R}_{\mathcal{S}_{\parallel}} c_{R,\text{Ta}\pm\sigma}^{\dagger} &\rightarrow c_{R,\text{Ta}\mp\sigma}^{\dagger} \\ \mathcal{R}_{\mathcal{S}_{\parallel}} c_{R,\text{Ni}\sigma}^{\dagger} &\rightarrow c_{R,\text{Ni}\sigma}^{\dagger}. \end{aligned} \quad (7)$$

It follows that, due to the invariance under $\mathcal{R}_{\mathcal{S}_{\perp}}$ the Γ -point hybridization identically vanishes

$$\Psi_{\pm} = \sum_{\sigma} \langle c_{k=0,\text{Ta}\pm,\sigma}^{\dagger} c_{k=0,\text{Ni},\sigma} \rangle = \frac{1}{N^2} \sum_{R,R'} \langle c_{R,\text{Ta}\pm,\sigma}^{\dagger} c_{R',\text{Ni},\sigma} \rangle = \frac{1}{N} \sum_{R} \langle c_{R,\text{Ta}\pm,\sigma}^{\dagger} c_{0,\text{Ni},\sigma} \rangle \quad (8)$$

$$\Psi_{\pm} = \mathcal{R}_{\mathcal{S}_{\perp}} \Psi_{\pm} = -\frac{1}{N} \sum_{R} \langle c_{-R-a,\text{Ta}\pm,\sigma}^{\dagger} c_{0,\text{Ni},\sigma} \rangle = -\Psi_{\pm} = 0. \quad (9)$$

Moreover, invariance under $\mathcal{R}_{\mathcal{S}_{\parallel}}$ implies $\Psi_{+} = \Psi_{-}$.

The Hamiltonian H_{int} contains intra- and inter-chain density-density interaction terms

$$H_{int} = \sum_{\sigma\sigma'} \sum_{\alpha\beta} \sum_{RR'} U_{\alpha\beta}^{\sigma\sigma'}(R - R') c_{R\alpha\sigma}^{\dagger} c_{R\alpha\sigma} c_{R'\beta\sigma'}^{\dagger} c_{R'\beta\sigma'}. \quad (10)$$

We consider long-range interaction potentials decaying as $|R|^{-1}$, and parametrized by the intracell interaction strengths

$$U_{\alpha\alpha}^{\sigma\sigma'}(R) = U_{\alpha} \frac{a}{|R| + a} [\delta_{\sigma,\sigma'} (1 - \delta_{R,0}) + \delta_{\sigma-\sigma'}], \quad (11)$$

and

$$U_{\text{Ta}\pm,\text{Ni}}^{\sigma\sigma'}(R) = V \frac{a}{|R| + |R + a|}. \quad (12)$$

We neglect $\text{Ta}_{+} - \text{Ta}_{-}$ interaction $U_{\text{Ta}_{+},\text{Ta}_{-}} = 0$.

We solve the interacting model by considering the Hartree-Fock mean-field decoupling in the particle-hole channel imposing the translational invariance of the chain. We define the particle-hole amplitudes

$$\Delta_{\alpha\beta}^{\sigma}(k) \equiv \langle c_{k\alpha\sigma}^{\dagger} c_{k\beta\sigma} \rangle \quad (13)$$

which, upon decoupling of the interaction, are self-consistently determined by the ground state of the Hamiltonian

$$H_{HF} = H_0 + \sum_{\alpha\beta} \sum_{\sigma} c_{k\alpha\sigma}^{\dagger} c_{k\beta\sigma} W_{\alpha\beta}^{\sigma}(k) + \text{h.c.} \quad (14)$$

where the effect of the interaction is included in the self-consistent fields

$$W_{\alpha\beta}^{\sigma}(k) \equiv - \sum_{k'} U_{\alpha\beta}^{\sigma\sigma}(k - k') [\Delta_{\alpha\beta}^{\sigma}(k')]^*. \quad (15)$$

Notice that the divergent of the Hartree term is absorbed into a redefinition of the chemical potential to fix the average number of electron per unit cell, and is not included in the self-consistent Hamiltonian. To carry out the momentum integration in Eq. 15, we smear out the $q \rightarrow 0$ singularity of the interaction by introducing a tiny exponential cut-off, and check convergence with respect to the latter.

II. CHARGE AND CURRENT DENSITY

In this section, we analyse the charge and current density in the CD and LC excitonic phases discussed in the main text.

Charge Density

The charge density reads

$$\rho(x, y) = \sum_{\alpha\beta} \sum_{RR'} \sum_{\sigma} w_{R,\alpha}(x, y) w_{R',\beta}(x, y) \langle c_{R\alpha\sigma}^{\dagger} c_{R'\beta\sigma} \rangle = \sum_{\alpha} \rho_{\alpha\alpha}(x, y) + \sum_{\alpha\neq\beta} \rho_{\alpha\neq\beta}(x, y) \quad (16)$$

where $\rho_{\alpha\alpha}(x, y)$ are the diagonal component. The off-diagonal components further split into $\text{Ta}_+ - \text{Ta}_-$ and $\text{Ta}_{\pm} - \text{Ni}$ contributions as $\rho_{\alpha\neq\beta}(x, y) = \rho_{\text{Ta}_+,\text{Ta}_-}(x, y) + \rho_{\text{Ta},\text{Ni}}(x, y)$ with

$$\rho_{\alpha,\alpha}(x, y) = \frac{1}{2} \sum_{R,R'} \sum_{\sigma} w_{R,\alpha}(x, y) w_{R',\alpha}(x, y) \left[\langle c_{R\alpha\sigma}^{\dagger} c_{R'\alpha\sigma} \rangle + c.c. \right] \quad (17)$$

$$\rho_{\text{Ta}_+,\text{Ta}_-}(x, y) = \sum_{R,R'} \sum_{\sigma} w_{R,\text{Ta}_+}(x, y) w_{R',\text{Ta}_-}(x, y) \left[\langle c_{R\text{Ta}_+\sigma}^{\dagger} c_{R'\text{Ta}_-\sigma} \rangle + c.c. \right] \quad (18)$$

$$\rho_{\text{Ta},\text{Ni}}(x, y) = \sum_{\alpha=\text{Ta}_{\pm}} \sum_{R,R'} \sum_{\sigma} w_{R,\alpha}(x, y) w_{R',\text{Ni}}(x, y) \left[\langle c_{R\alpha\sigma}^{\dagger} c_{R'\text{Ni}\sigma} \rangle + c.c. \right] \quad (19)$$

We analyse the symmetry with respect to the reflections. Let us first consider the symmetry with respect to \mathcal{S}_{\perp} , and compute the charge asymmetry

$$\delta_{\perp}(x, y) = \rho(x, y) - \rho(-x, y). \quad (20)$$

with

$$\rho(-x, y) = \sum_{\alpha} \rho_{\alpha\alpha}(-x, y) + \rho_{\text{Ta}_+,\text{Ta}_-}(-x, y) + \rho_{\text{Ta},\text{Ni}}(-x, y). \quad (21)$$

By exploiting the translational invariance, i.e. $\langle c_{R\alpha\sigma} c_{R'\beta\sigma} \rangle = \langle c_{R+R''\alpha\sigma} c_{R'+R''\beta\sigma} \rangle$ for any R'' , we get

- diagonal component

$$\rho_{\alpha\alpha}(x, y) - \rho_{\alpha\alpha}(-x, y) = \sum_{RR'} \sum_{\sigma} w_{R\alpha}(x, y) w_{R'\alpha}(x, y) \text{Re} \left[\langle c_{(R-R')\alpha\sigma}^{\dagger} c_{0\alpha\sigma} \rangle - \langle c_{(R'-R)\alpha\sigma}^{\dagger} c_{0\alpha\sigma} \rangle \right] \quad (22)$$

- off-diagonal components

$$\rho_{\text{Ta}_+,\text{Ta}_-}(x, y) - \rho_{\text{Ta}_+,\text{Ta}_-}(-x, y) = \sum_{RR'} \sum_{\sigma} w_{R\text{Ta}_+}(x, y) w_{R'\text{Ta}_-}(x, y) \text{Re} \left[\langle c_{(R-R')\text{Ta}_+\sigma}^{\dagger} c_{0\text{Ta}_-\sigma} \rangle - \langle c_{(R'-R)\text{Ta}_+\sigma}^{\dagger} c_{0\text{Ta}_-\sigma} \rangle \right] \quad (23)$$

$$\rho_{\text{Ta},\text{Ni}}(x, y) - \rho_{\text{Ta},\text{Ni}}(-x, y) = \sum_{\alpha=\text{Ta}_{\pm}} \sum_{RR'} \sum_{\sigma} w_{R\alpha}(x, y) w_{R'\text{Ni}}(x, y) \text{Re} \left[\langle c_{(R-R')\alpha\sigma}^{\dagger} c_{0\text{Ni}\sigma} \rangle + \langle c_{(R'-R-a)\alpha\sigma}^{\dagger} c_{0\text{Ni}\sigma} \rangle \right] \quad (24)$$

It follows that the charge is symmetric with respect to reflections about the $x = 0$ plane if the intra- and inter-orbital amplitudes obey

$$\begin{aligned} \text{Re} \langle c_{R\alpha\sigma}^{\dagger} c_{0\alpha\sigma} \rangle &= \text{Re} \langle c_{-R\alpha\sigma}^{\dagger} c_{0\alpha\sigma} \rangle \\ \text{Re} \langle c_{R\text{Ta}_+\sigma}^{\dagger} c_{0\text{Ta}_-\sigma} \rangle &= \text{Re} \langle c_{-R\text{Ta}_+\sigma}^{\dagger} c_{0\text{Ta}_-\sigma} \rangle \quad \longrightarrow \quad \delta_{\perp}(x, y) = 0 \\ \text{Re} \langle c_{R\text{Ta}_{\pm}\sigma}^{\dagger} c_{0\text{Ni}\sigma} \rangle &= -\text{Re} \langle c_{-R-a\text{Ta}_{\pm}\sigma}^{\dagger} c_{0\text{Ni}\sigma} \rangle \end{aligned} \quad (25)$$

Let us consider now the reflection with respect to the longitudinal plane

$$\delta_{\parallel}(x, y) = \rho(x, y) - \rho(x, -y) \quad (26)$$

- diagonal components

$$\begin{aligned} \sum_{\alpha=\text{Ta}_\pm} \rho_{\alpha\alpha}(x, y) - \rho_{\alpha\alpha}(x, -y) &= \sum_{RR'} [w_{R\text{Ta}_+}(x, y)w_{R'\text{Ta}_+}(x, y) - w_{R\text{Ta}_-}(x, y)w_{R'\text{Ta}_-}(x, y)] \times \\ &\quad \times \text{Re} [\langle c_{(R-R')\text{Ta}_\pm\sigma}^\dagger c_{0\text{Ta}_\pm\sigma} \rangle - \langle c_{(R-R')\text{Ta}_\mp\sigma}^\dagger c_{0\text{Ta}_\mp\sigma} \rangle] \end{aligned} \quad (27)$$

$$\rho_{\text{NiNi}}(x, y) - \rho_{\text{NiNi}}(x, -y) = 0$$

- off-diagonal components

$$\rho_{\text{Ta}_+\text{Ta}_-}(x, y) - \rho_{\text{Ta}_+\text{Ta}_-}(x, -y) = \sum_{RR'} w_{R\text{Ta}_+}(x, y)w_{R'\text{Ta}_-}(x, y) \text{Re} [\langle c_{(R-R')\text{Ta}_+\sigma}^\dagger c_{0\text{Ta}_-\sigma} \rangle - \langle c_{(R-R')\text{Ta}_-\sigma}^\dagger c_{0\text{Ta}_+\sigma} \rangle] \quad (28)$$

$$\rho_{\text{Ta}_\pm\text{Ni}}(x, y) - \rho_{\text{Ta}_\pm\text{Ni}}(x, -y) = \sum_{RR'} w_{R\text{Ta}_\pm}(x, y)w_{R'\text{Ta}_\mp}(x, y) \text{Re} [\langle c_{(R-R')\text{Ta}_\pm\sigma}^\dagger c_{0\text{Ni}\sigma} \rangle - \langle c_{(R-R')\text{Ta}_\mp\sigma}^\dagger c_{0\text{Ni}\sigma} \rangle] \quad (29)$$

It follows that the charge is symmetric with respect to reflections about the $y = 0$ plane if the intra- and inter-orbital amplitudes obey

$$\begin{aligned} \text{Re} \langle c_{R\text{Ta}_\pm\sigma}^\dagger c_{0\text{Ta}_\pm\sigma} \rangle &= \text{Re} \langle c_{R\text{Ta}_\mp\sigma}^\dagger c_{0\text{Ta}_\mp\sigma} \rangle \\ \text{Re} \langle c_{R\text{Ta}_+\sigma}^\dagger c_{0\text{Ta}_-\sigma} \rangle &= \text{Re} \langle c_{-R\text{Ta}_+\sigma}^\dagger c_{0\text{Ta}_-\sigma} \rangle \quad \rightarrow \quad \delta_{\parallel}(x, y) = 0 \\ \text{Re} \langle c_{R\text{Ta}_\pm\sigma}^\dagger c_{0\text{Ni}\sigma} \rangle &= \text{Re} \langle c_{R\text{Ta}_\mp\sigma}^\dagger c_{0\text{Ni}\sigma} \rangle \end{aligned} \quad (30)$$

In Fig. 2 (first row) we show the real parts of the diagonal and off-diagonal amplitudes $\Delta_\sigma^{\alpha\beta}(R) \equiv \langle c_{R\alpha\sigma}^\dagger c_{0\beta\sigma} \rangle$ for the CD $\varphi = 0$ and LC $\varphi = \pi/2$ excitonic insulating phases. We see that for the CD phase the charge density is not invariant under both reflection symmetries, i. $\delta_{\perp} \neq 0$ and $\delta_{\parallel} \neq 0$. In particular, symmetry breaking is evident in the off-diagonal components, $(\text{Ta}_+, \text{Ta}_-)$ and $(\text{Ta}_\pm, \text{Ni})$. We further notice that the $(\text{Ta}_+, \text{Ta}_-)$ component of the charge density transforms in the same way under both symmetries. Moreover, we see that the (Ta_+, Ni) and (Ta_-, Ni) components are related by

$$\Delta_\sigma^{\text{Ta}_-, \text{Ni}}(R) = -\Delta_\sigma^{\text{Ta}_+, \text{Ni}}(-R - a) \quad (31)$$

so that the conditions 24 and 29 becomes equivalent, meaning that also the (Ta_+, Ni) and (Ta_-, Ni) components transform in the same way under both symmetry. As a result, charge density remains invariant under the simultaneous action of the two reflections, leading to the charge density distribution for the CD phase sketched in the main text. By looking at the same quantities for the LC phase, it is immediate to check that, for this phase, the charge density preserves both reflection symmetries.

Current Density

We now consider the current distribution. The current density operator is defined by taking the variation of the Hamiltonian with respect to a probe field $\vec{A}(\vec{r})$

$$\vec{j}(\vec{r}) = - \left. \frac{\delta H(\vec{A})}{\delta \vec{A}(\vec{r})} \right|_{\vec{A}=0} \quad (32)$$

Since we are considering a tight-binding model, the probe field enter through Peierls phases

$$H(\vec{A}) = \sum_{RR'} \sum_{\alpha\beta} t_{RR'}^{\alpha\beta} \exp \left[-i \frac{e}{\hbar} \int_{\vec{r}_{R'\beta}}^{\vec{r}_{R\alpha}} d\vec{r} \cdot \vec{A}(\vec{r}) \right] c_{R\alpha}^\dagger c_{R'\beta} + H_{int} \quad (33)$$

where $\int_{\vec{r}_{R'\beta}}^{\vec{r}_{R\alpha}} d\vec{r} \cdot \vec{A}(\vec{r})$ is a line integral along a straight line connecting the Wannier centers $R'\beta$ and $R\alpha$. To proceed, it is custom to assume that the probe field varies smoothly along the integration line, so that one can approximate

$$\int_{\vec{r}_{R'\beta}}^{\vec{r}_{R\alpha}} d\vec{r} \cdot \vec{A}(\vec{r}) \simeq \vec{A}_{R\alpha, R'\beta} \cdot [\vec{r}_{R\alpha} - \vec{r}_{R'\beta}]$$

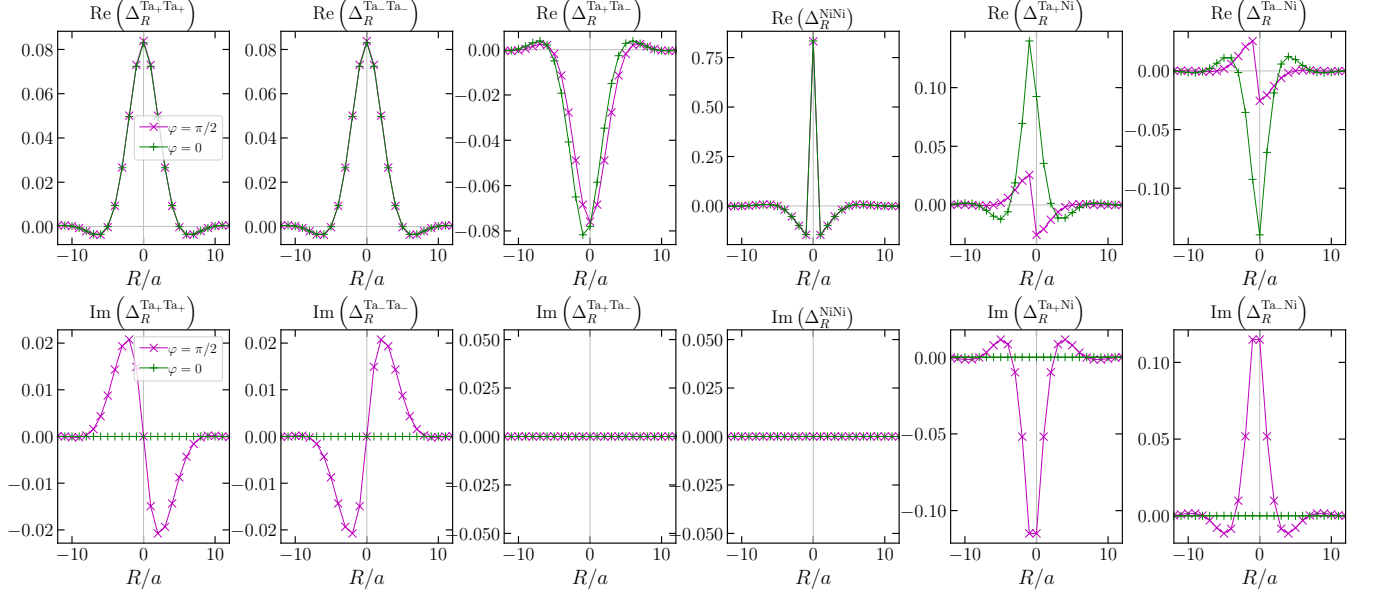


Figure 2. Real (first row) and imaginary (second row) parts of the amplitudes $\Delta_{\sigma}^{\alpha\beta}(R) \equiv \langle c_{R\alpha\sigma}^{\dagger} c_{0\beta\sigma} \rangle$ in the CD (green plus symbols), and LC ($\varphi = \pi/2$) phase, magenta cross symbols.

where $\vec{A}_{R\alpha,R'\beta}$ is the vector potential evaluated at the mid point $\vec{r}_{R\alpha,R'\beta} = \frac{\vec{r}_{R\alpha} + \vec{r}_{R'\beta}}{2}$ of the straight line. In doing so, the functional derivative leads to a current density defined on the mid-point of links between lattice sites as

$$\vec{j}(\vec{r}) = -\frac{e}{\hbar} \sum_{RR'} \sum_{\alpha\beta} \delta(\vec{r} - \vec{r}_{R\alpha,R'\beta}) [\vec{r}_{R\alpha} - \vec{r}_{R'\beta}] 2\text{Im} \left(t_{RR'}^{\alpha\beta} \langle c_{R\alpha}^{\dagger} c_{R'\beta} \rangle \right) = \sum_{RR'} \sum_{\alpha\beta} \delta(\vec{r} - \vec{r}_{R\alpha,R'\beta}) \vec{u}_{R\alpha,R'\beta} I_{RR'}^{\alpha\beta} \quad (34)$$

where $\vec{u}_{R\alpha,R'\beta} = \frac{\vec{r}_{R\alpha} - \vec{r}_{R'\beta}}{|\vec{r}_{R\alpha} - \vec{r}_{R'\beta}|}$ is the link unit vector, and $I_{RR'}^{\alpha\beta}$ is the intensity current on the link. Since the intensity current proportional to the hopping, only nearest-neighboring links have non zero current. In the following, we list the expressions for the currents amplitude for the nearest neighboring links in the absence of external fields for which the hopping amplitudes are real. The summation over spin is understood.

$$\vec{j}_{R,R-a}^{\text{Ta}\pm\text{Ta}\pm} = -\frac{e}{\hbar} \hat{x} a 2 t_{R,R-a}^{\text{Ta}\pm\text{Ta}\pm} \text{Im}(\langle c_{a\text{Ta}\pm\sigma}^{\dagger} c_{0\text{Ta}\pm\sigma} \rangle) \quad (35)$$

$$\vec{j}_{R,R-a}^{\text{NiNi}} = -\frac{e}{\hbar} \hat{x} a 2 t_{R,R-a}^{\text{NiNi}} \text{Im}(\langle c_{a\text{Ni}\sigma}^{\dagger} c_{0\text{Ni}\sigma} \rangle) \quad (36)$$

$$\vec{j}_{R,R}^{\text{Ta}\pm\text{Ni}} = -\frac{e}{\hbar} (-a\hat{x} - b\hat{y}) t_{R,R}^{\text{Ta}\pm,\text{Ni}} \text{Im}(\langle c_{0\text{Ta}\pm\sigma}^{\dagger} c_{0\text{Ni}\sigma} \rangle) \quad (37)$$

$$\vec{j}_{R,R-a}^{\text{Ta}\pm\text{Ni}} = -\frac{e}{\hbar} (a\hat{x} - b\hat{y}) t_{R,R-a}^{\text{Ta}\pm,\text{Ni}} \text{Im}(\langle c_{a\text{Ta}\pm\sigma}^{\dagger} c_{0\text{Ni}\sigma} \rangle) \quad (38)$$

where \hat{x} and \hat{y} are the x, y unit vectors and a and b are the lattice parameters.

In Fig. 2 (second row) we show the imaginary parts of the amplitudes $\Delta_{\sigma}^{\alpha\beta}(R)$. In the CD phase, all the amplitudes are purely real so that the ground state current is always zero. On the contrary, in the LC phase the imaginary parts leads to a pattern of currents which, by considering the signs of the hoppings, coincides with the pattern sketched in the main text.

III. ELECTRON PHONON COUPLING AND STABILITY OF THE LC PHASE

We now consider the full Hamiltonian including the electron-phonon coupling

$$H = H_{el} + H_{ph} + H_{ph-el}. \quad (39)$$

We use the standard mean-field decoupling $|\Psi\rangle = |\Psi_{el}\rangle |\Psi_{ph}\rangle$ which leads to a set of coupled Schrödinger equations for the electronic and phononic wave functions

$$\tilde{H}_{el} |\Psi_{el}\rangle = E_{el} |\Psi_{el}\rangle \quad (40)$$

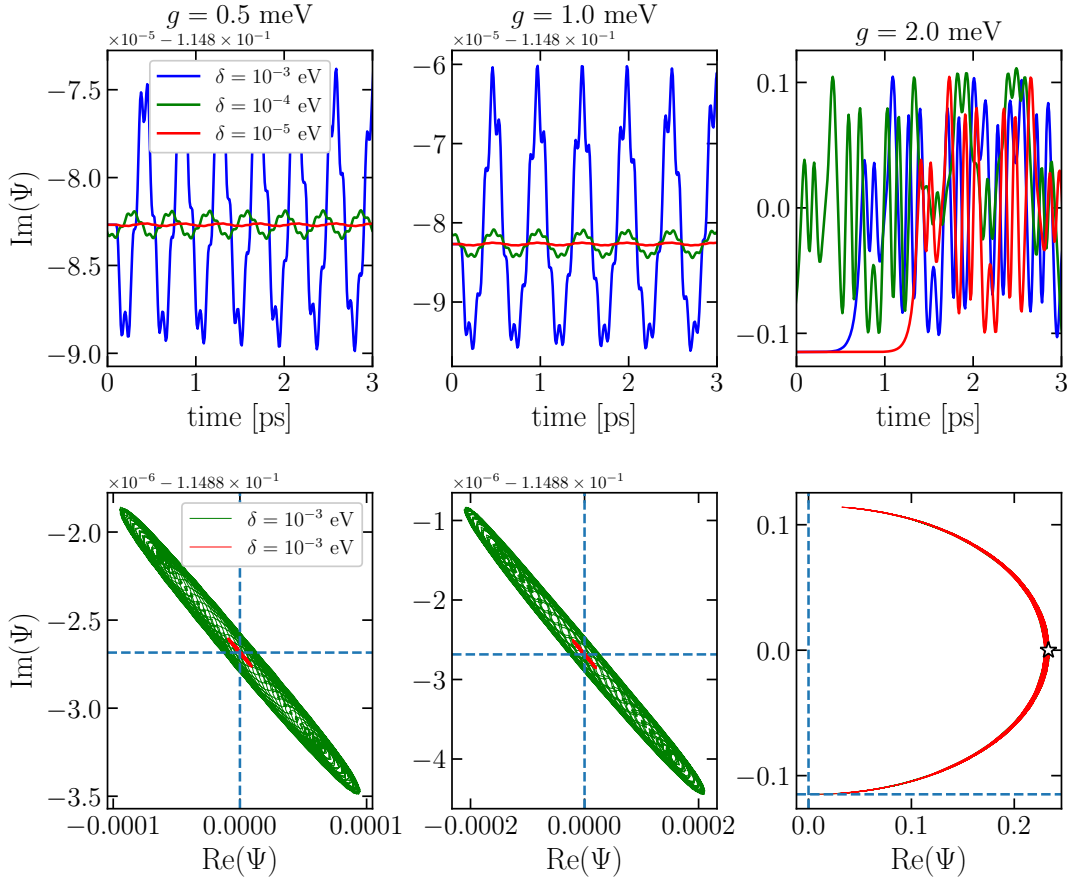


Figure 3. (First row) Dynamics of the imaginary part of the order parameter for different values of the perturbation δ and electron-phonon coupling. (Second row) trajectories in the $(\text{Re}(\Psi), \text{Im}\Psi)$ complex plane for different values of g and $\delta = 10^{-4}$ eV (green line) and $\delta = 10^{-5}$ eV (red lines). Vertical and horizontal dashed lines mark the equilibrium undistorted LC solution. In the rightmost panel the star symbol indicates the structurally distorted equilibrium solution.

$$\tilde{H}_{ph}|\Psi_{ph}\rangle = E_{ph}|\Psi_{ph}\rangle \quad (41)$$

where the effective Hamiltonians read

$$\tilde{H}_{ph} = H_{ph} + \langle \Psi_{el} | H_{el-ph} | \Psi_{el} \rangle \quad \text{and} \quad \tilde{H}_{el} = H_{el} + \langle \Psi_{ph} | H_{el-ph} | \Psi_{ph} \rangle.$$

We notice that the effective electronic Hamiltonian depends on the electron-phonon coupling only through the static distortion of the mode $\langle X_{R\alpha} \rangle$

$$\tilde{H}_{el} = H_{el} + g \sum_{\alpha} \langle X_{R\alpha} \rangle \left(c_{R\text{Ni}\sigma}^{\dagger} c_{R\alpha\sigma} + c_{R\text{Ni}\sigma}^{\dagger} c_{R-a\alpha\sigma} + \text{h.c.} \right).$$

It follows that, as mentioned in the main text, within the mean-field decoupling, any undistorted solution of the electron-phonon problem is equivalent to the $g = 0$ case.

To see the effects of the electron-phonon coupling onto the undistorted phase, we check fluctuations about the equilibrium mean-field solution. To do so we supplement the Hamiltonian with a small delta-like time-dependent perturbation that couples with the phonon displacement as

$$H \rightarrow H(t) = H + \lambda(t) \sum_R (X_{R\text{Ta}_+} - X_{R\text{Ta}_-}) \quad (42)$$

with $\lambda(t) = \delta \exp(-(t - t_0)^2/2\tau^2)$, and study the dynamics with time-dependent Hartree-Fock. We choose τ much smaller than the characteristic period of the order parameter oscillations and study the dynamics for different values of δ . In Fig. 3 (first row), we show the dynamics of the order parameter of the LC phase for different perturbations

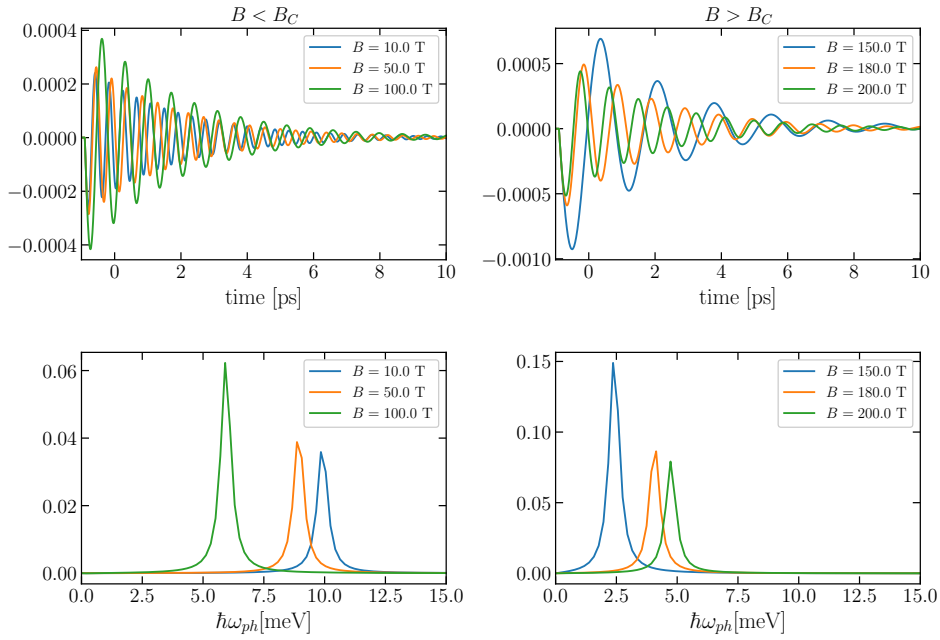


Figure 4. (First row) Dynamics of the displacements for different values of the applied fields in the structurally distorted (left) and the LC phase for $g = 3$ meV. (Second row) Corresponding phonon spectral functions.

δ and increasing electron-phonon coupling. For $g = 0.5$ meV and $g = 1.0$ meV, we observe small oscillations around the equilibrium values with amplitude proportional to the perturbation strength. In contrast, for $g = 2$ meV the perturbation induces large oscillation with amplitude independent of the perturbation strength. Moreover, the order parameter does not oscillates around the equilibrium value clearly signalling the instability of the LC solution due to the large electron-phonon coupling g . This can be better appreciated by looking at the order parameter trajectories in the complex plane (second row), clearly showing that for small g the order parameter oscillates around the equilibrium undistorted solution. On the contrary, for $g = 2$ meV the order parameter escapes from the undistorted solution and starts to oscillate around the distorted solution which is the only stable phase for this value of g .

IV. LATTICE DYNAMICS

We now describe the determination of the phonon frequency. We employ the same time-dependent perturbation of Eq. 42, and for all the cases in which a stable solution is found, we track the oscillation in time of the phonon displacement $\langle X_{\text{Ta}} \rangle(t)$. Therefore, we use the linear response theory to relate the mode oscillation to the phonon response function as

$$\langle X_{\text{Ta}} \rangle(t) = \langle X_{\text{Ta}} \rangle_0 + \int_{-\infty}^{+\infty} dt' \chi_{ph}(t-t') \lambda(t') \quad (43)$$

From Eq. 43, we extract the response function $\chi_{ph}(t-t')$, and compute its Fourier transform. Eventually, we determine the frequency of the mode by averaging the frequency over the spectral function $A_{ph}(\omega) = -\frac{1}{\pi} \text{Im} \chi_{ph}(\omega)$

$$\omega_{ph} = \frac{\int d\omega \omega A_{ph}(\omega)}{\int d\omega q A_{ph}(\omega)} \quad (44)$$

In Fig.4, we show few examples of lattice dynamics across the magnetic-field induced monoclinic-to-orthorombic distortion.

[1] G. Mazza, M. Rösner, L. Windgätter, S. Latini, H. Hübener, A. J. Millis, A. Rubio, and A. Georges, *Phys. Rev. Lett.* **124**, 197601 (2020).